

Investigation on microwave absorption capacity of nanocomposites based on metal oxides and graphene

Pallab Bhattacharya · Chapal Kumar Das

Received: 25 September 2012 / Accepted: 5 December 2012 / Published online: 13 December 2012
© Springer Science+Business Media New York 2012

Abstract Graphene and its nanocomposites were prepared via solution mixing process. Graphene based polymer nanocomposites were prepared by two step process. Firstly, graphene/poly(3-methyl thiophene)(PMT)/BaTiO₃ nanocomposite was prepared by in situ chemical oxidation polymerization technique. In the second step these nanocomposites were dispersed in thermoplastic polyurethane (TPU) matrix by solution blending process. All the four nanocomposites in TPU [30 % modified graphene (P1), 30 % Poly(3-methyl thiophene) (P2), 30 % graphene/PMT/BaTiO₃ (P3) and 15 % graphene/PMT/BaTiO₃ + 15 % Fe₃O₄ (P4)] were analyzed by different analytical techniques like X-ray diffraction (XRD), scanning electron microscopy (SEM), Energy-dispersive X-ray spectroscopy (EDX) and transmission electron microscopy (TEM). Microwave absorbing property was measured by Agilent vector network analyzer (ENA E5071C) in the X-band region (8–12 GHz). Microwave absorption result was interpreted with the help of complex permittivity and permeability of the prepared materials. Matching of both dielectric loss and magnetic loss is essential for an effective radar absorbing material (RAM). P1, P2, P3 and P4 showed the maximum return loss of -14.37, -9.3, -30.02 and -47.59 dB respectively. Thermal stability of the RAMs was determined by the help of thermogravimetric analysis (TGA) instrument. Among the all, P4 showed better thermal property. All results support their use as RAM in different field.

1 Introduction

Since 1930s researchers are showing their interest on RADAR absorbing materials (RAMs) or Microwave absorbing materials due to their potential commercial and military application [1]. RAMs are widely known for their capacity of suppressing microwave radiations. RAMs are also can be used to reduce the radar cross section (RCS) and to shield the electromagnetic interference (EMI) problems [2, 3]. Microwave is an electromagnetic radiation consisting of two components, electric and magnetic. Hence to absorb microwave radiation, a RAM should have the capability of cancelling out both the electric and magnetic components of the microwave radiation. An excellent RAM should be light weight and thin which can also cover a broad frequency range. To serve these purpose materials like ferroelectric [4], ferromagnetic [5] conducting materials [6–8] and their combination [9] has been used. Graphene can be used as an excellent microwave absorbing material [10] due to its sheet like structure [11], high surface area (up to 2,600 m² g⁻¹), high electrical conductivity (up to 6,000 S cm⁻¹) and good thermal conductivity (5,000 W m⁻¹ K⁻¹). Graphene also has highest Young's modulus up to 1,000 GPa [12]. Many microwave studies have already been reported with carbon nanotube nanocomposites [13–15] but with the nanocomposites of graphene it is very few. It has already been reported that single CNT is not good enough for microwave absorption but its composite has the ability to play a decent role into microwave absorption [16, 17]. The picture is same for graphene and its composites. In one such work, Xiaohong Wang et al. [18] reported the reflection loss of -6.9 dB for chemically reduced graphene whereas; Liang et al. [19] reported the reflection loss of -21 dB for graphene/epoxy composite in X-band region. Yong Zhang et al. reported

P. Bhattacharya · C. K. Das (✉)
Materials Science Centre, Indian Institute of Technology,
Kharagpur 721302, West Bengal, India
e-mail: chapal12@yahoo.co.in

the effect of loading and thickness of graphene, on the microwave absorption property of graphene/PEO nanocomposites [12]. The combine effect of graphene with some magnetic component also been studied, for the superior microwave absorption property [20] but still there is a lot of scope to tune the nanocomposite of graphene with respect to their component, morphology, loading, thickness of the material etc. Although graphene can act as a microwave absorbing material, but an effective absorption can only be achieved if a combination of conducting, dielectric and magnetic materials are used. The present study targeted the fabrication of graphene and metal oxide based RAMs, in combination with conducting polymer (polythiophene), magnetic particle (Fe_3O_4) and dielectric material (BaTiO_3), for superior microwave absorption in the X-band region. Fe_3O_4 , a member of spinel family, was used because it has low toxicity and great stability at high temperature [21, 22]. Fe_3O_4 is also a promising material for showing excellent microwave absorption at lower frequencies, which is particularly related to magnetic loss [23]. Among the conducting polymers, poly(3-methyl thiophene) (PMT) was taken due to its environmental stability and high electrical conductivity [24, 25]. The matrix used for the preparation of different RAMs is thermoplastic polyurethane (TPU). Total filler percentage was maintained at 30 % and the thicknesses of the RAMs were 2 mm. The ferroelectric phase, magnetic phase and conducting phase coexist in one material; magneto-electric properties and the other coupling are expected due to interaction between magnetization and electric polarization. Microwave absorption study was done by using Agilent vector network analyzer (ENA E5071C) in the X-band region (8–12 GHz).

2 Experimental work

2.1 Materials

Graphene was obtained from Sinocarbon Materials Technology Co. Ltd. China. Chloroform (CHCl_3), methanol (CH_3OH), tetrahydrofuran ($\text{C}_4\text{H}_8\text{O}$) and acetone (CH_3COCH_3) were purchased from Merck, India. 3-methyl-thiophene was purchased from Spectrochem Private Limited, India. Ferric chloride (FeCl_3), barium titanate (BaTiO_3), magnetite (Fe_3O_4) and cetyltrimethylammonium bromide (CTAB) were purchased from Loba Chemie Private Limited, India. All the chemicals and materials were used as purchased without any purification unless specified. The TPU utilized for developing RAMs belong to commercial medical grade aliphatic, polyether (Tecoflex VR EG 80A injection grade) procured from Lubrizol Advanced Materials, Thermedics TM Inc. Polymer Products, USA. Tecoflex EG 80A (around 35 % of hard segments) has shore hardness of 72A,

specific gravity = 1.04, and its constituent formulation contains methylene bis(cyclohexyl) diisocyanate (HMDI) as hard segment, and polytetramethylene oxide (PTMO) as soft segment (molecular weight = 1,000 g/mol), and chain extender 1, 4-butane di-ol (BD).

2.2 Composition of the nanocomposites

Four different TPU based nanocomposites were prepared with various combinations of fillers. Details of the samples were given in Table 1. The nanocomposites were prepared by two step process. Firstly, PMT and graphene/PMT/ BaTiO_3 nanocomposite were prepared by the following method. Then these were dispersed in TPU matrix for the preparation of nanocomposite.

2.3 Modification of graphene

In order to address the compatibility issue, with the TPU matrix, surface modification of graphene was carried out using mixed acid ($\text{HNO}_3/\text{H}_2\text{SO}_4$). At first graphene was treated with a solution of H_2SO_4 and HNO_3 (weight ratio of H_2SO_4 to HNO_3 was 3:1). Here the weight ratio of the mixed acid to graphene was 200:1. Then the whole solution was stirred at 80 °C for 24 h to get acid modified graphene. After that the solution was centrifuged and washed with distilled water and ethanol, several times. The prepared black coloured solution was dried at 100 °C for 12 h to get the acid modified graphene.

2.4 Preparation of graphene/PMT/ BaTiO_3 nanocomposite

A typical in situ chemical oxidative polymerization was carried out to synthesize nanocomposites and the process was shown in Fig. 1 by a schematic presentation. In 100 ml CHCl_3 , 0.2 gm modified graphene was added and sonicated for 30 min with CTAB at room temperature. To this well dispersed solution, 0.8 gm BaTiO_3 was added and sonicated for 20 min. To this suspension, 50 ml CHCl_3 containing 2 gm FeCl_3 was added and sonicated for 10 min. Subsequently, 50 ml CHCl_3 containing 1 ml 3-methyl-thiophene monomer was added drop wise to the above solution and further sonicated for 30 min at room

Table 1 Composition used for RAMs preparation

Sample code	Composition in 70 % TPU
P1	Modified graphene (30 %)
P2	Poly(3-methyl thiophene) (30 %)
P3	Graphene/PMT/ BaTiO_3 (30 %)
P4	Graphene/PMT/ BaTiO_3 + Fe_3O_4 (15 + 15 %)

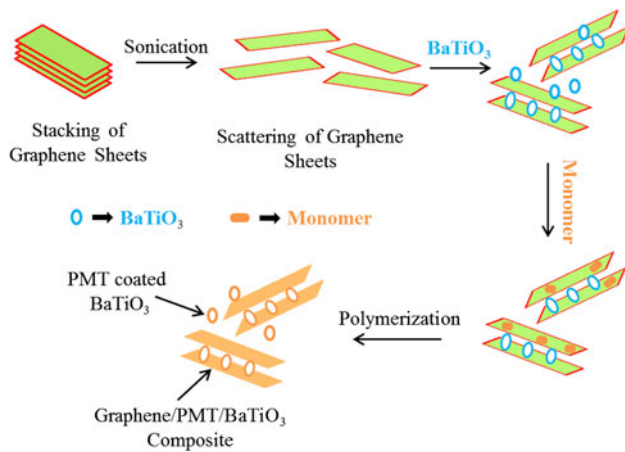


Fig. 1 Reaction scheme for preparation of graphene/PMT/BaTiO₃ composite

temperature. The whole reaction mixture was stirred in argon atmosphere for 24 h. The resulting reddish-black powder was precipitated in methanol, filtered with a Buchner funnel and thoroughly washed with methanol, hydrochloric acid (0.1 M), distilled water and acetone for several times and vacuum dried at room temperature for 24 h to get the desired graphene/PMT/BaTiO₃ nanocomposite. Pure poly (3-methyl-thiophene) (PMT) was synthesized, following the above mentioned procedure, in absence of graphene and BaTiO₃.

2.5 Preparation of microwave test plate

For the preparation of TPU based nanocomposites, TPU was dissolved in 200 ml THF at 60 °C by stirring it for overnight and then required filler was added to it in desired ratios. After well dispersion of the fillers, solvent was evaporated to make the mixture highly concentrated. Then this concentrated mixture was poured on a petri dish and kept in oven at 70 °C for complete drying. When drying was completed the test samples were prepared by compression molding technique at 5 MPa pressure and 170 °C temperature. Aluminum sheet was used as metallic backing material of the developed RAMs. Four samples were prepared with 30 % loading of graphene, PMT, graphene/PMT/BaTiO₃ and graphene/PMT/BaTiO₃ + Fe₃O₄ (15 + 15 %). Thickness of the RAM was maintained to 2 mm. All the four samples were cut into desired rectangular shape of size 0.4 inch × 0.9 inch to fit into X-band waveguide for microwave measurements.

3 Characterization

The samples were characterized by X-ray diffraction (XRD), which was conducted on a Rigaku X-ray Diffractometer, ULTIMA III with Cu K α radiation ($\lambda = 1.5418 \text{ \AA}$). The

surface morphology and filler distribution was analysed by scanning electron microscopy (SEM, VEGA LSU, TESCAN). Energy-dispersive X-ray spectroscopy (EDX) attached to SEM, while EDX analysis was performed to understand their chemical constituents. Transmission electron microscopy (TEM) analysis was carried out by a JEOL JEM-2100 microscope, to analyse the dispersion state of the fillers in TPU matrix. The microwave characteristics were analysed by Agilent vector network analyser (ENA E5071C). Thermogravimetric analysis (TGA) was performed by using Dupont 2100 Thermogravimetric analyzer. The TGA measurements were conducted at a heating rate of 10 °C/min under Nitrogen atmosphere from 30 to 650 °C.

4 Results and discussion

4.1 XRD analysis

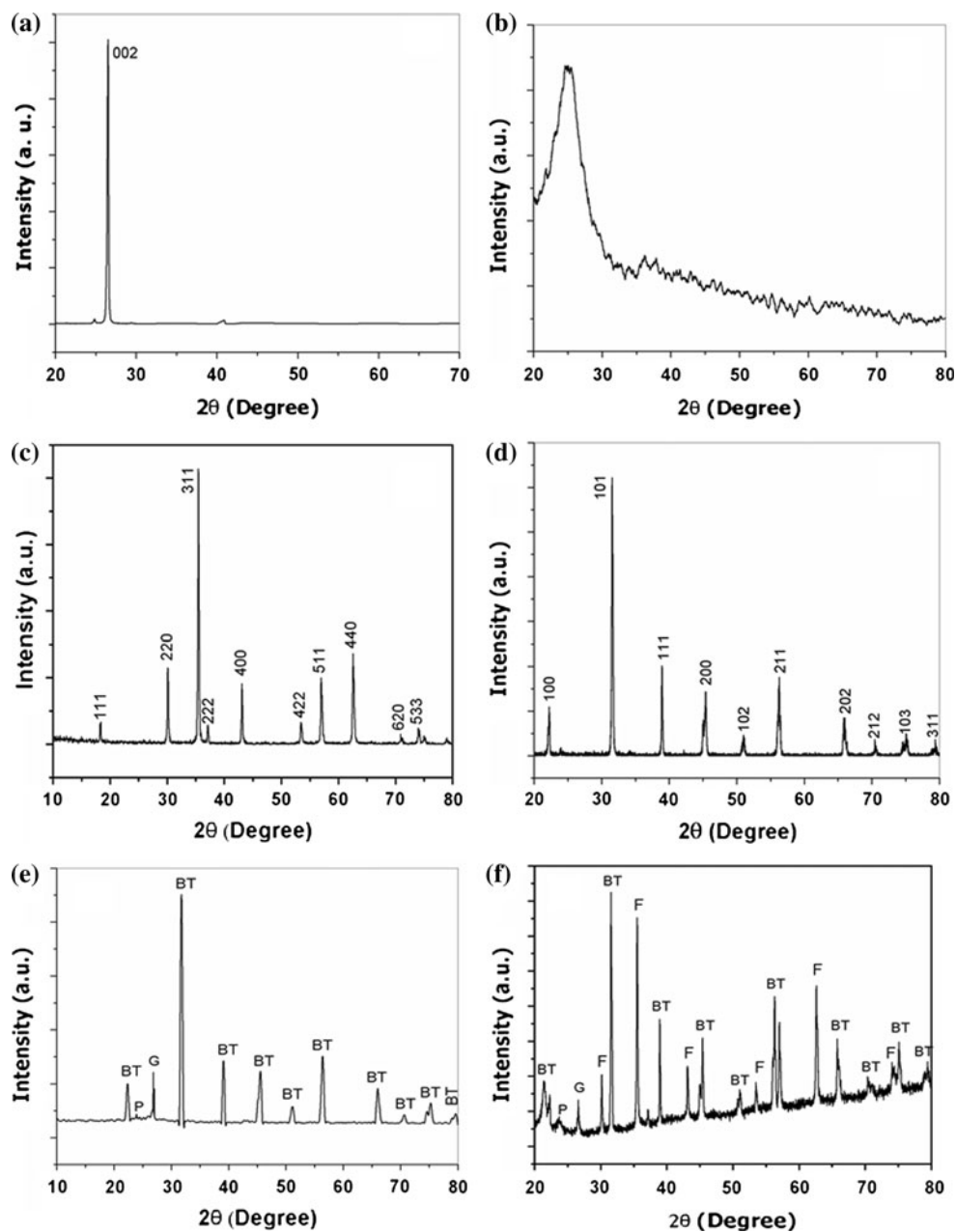
The XRD patterns of different nanocomposites are shown in Fig. 2a–f. Figure 2a showed the major peak at $2\theta = 26.39^\circ$ for graphene whereas Fig. 2b showed the peaks for PMT at $2\theta = 12.77^\circ$ and 25.07° . Figure 2c refers to the XRD pattern of Fe₃O₄. The major peaks available in Fe₃O₄ are perfectly matched with JCPDS analysis (No-75-1610) which shows that Fe₃O₄ belongs to Cubic system and have space group F3 dm [26]. Crystalline facets of Fe₃O₄ are (111), (220), (311), (220), (400), (422), (511), (400), (533) and (731) respectively. Characteristic peak for Fe₃O₄ was observed at $2\theta = 35.45^\circ$. Figure 2d showed the peak pattern for BaTiO₃ which is similar to the JCPDS, PDF no. 04-009-3215 [27]. JCPDS analysis confirmed the presence of crystalline facets (100), (101), (111), (200), (210), (211), (202), (212), (301) and (311) respectively. Characteristic peak obtained at $2\theta = 32.17^\circ$. Figure 2e represented the XRD analysis of graphene/PMT/BaTiO₃ nanocomposite and Fig. 2f represented the same in presence of Fe₃O₄. The graphene/PMT/BaTiO₃ nanocomposite contains the peak for graphene at $2\theta = 26.39^\circ$ and also the peak for both PMT and BaTiO₃ [28].

4.2 Morphological study

4.2.1 SEM analysis

Figure 3a–d showed the SEM images of graphene, PMT, BaTiO₃ and Fe₃O₄ respectively. Graphene has sheet like structure and consequently BaTiO₃ and Fe₃O₄ showing their particle nature. The formation of graphene/PMT/BaTiO₃ nanocomposite was further confirmed by SEM image showing in Fig. 3e where the BaTiO₃ particles sprinkled over the whole graphene sheet. Figure 3f–i represented the SEM images for the fractured cross-section,

Fig. 2 XRD analysis of **a** graphene [G], **b** PMT [P], **c** Fe_3O_4 [F], **d** BaTiO_3 [BT], **e** graphene/PMT/ BaTiO_3 nanocomposite and **f** graphene/PMT/ BaTiO_3 nanocomposite in presence of Fe_3O_4



generated by cryogenic treatment, of P1–P4 nanocomposites. Figure 3f showed the presence of graphene sheet in TPU. Figure 3h, i both proved the presence of particles in the nanocomposite. From the EDX study we can easily detect those particles. We have studied EDX for P3 and P4 showed in the Fig. 4. From the EDX results we proved that P3 contains Ba, Ti, C, S and O but P4 contains Fe also with those present in P3.

4.2.2 TEM analysis

For further morphological study of the nanocomposite, we have done TEM analysis and presented in the Fig. 5. TEM image of graphene/PMT/ BaTiO_3 nanocomposite confirms the

presence of agglomerated BaTiO_3 particle in the nanocomposite. P4 also showed the agglomeration of both BaTiO_3 and Fe_3O_4 particle. Fe_3O_4 particles may aggregate due to the magneto-dipole interaction among themselves [29]. The SAED (Selected Area Electron Diffraction) images of graphene and graphene/PMT/ BaTiO_3 nanocomposite are shown in Fig. 6. A perfect six membered ring pattern is observed in the SAED image of graphene. This is because of the crystalline nature of graphene. However, this ring pattern is absent in the SAED image of graphene/PMT/ BaTiO_3 . This is due to the coating of amorphous polymer in the crystalline graphene sheets. TEM images for both graphene/PMT/ BaTiO_3 nanocomposite and P4 showed the presence of particles.

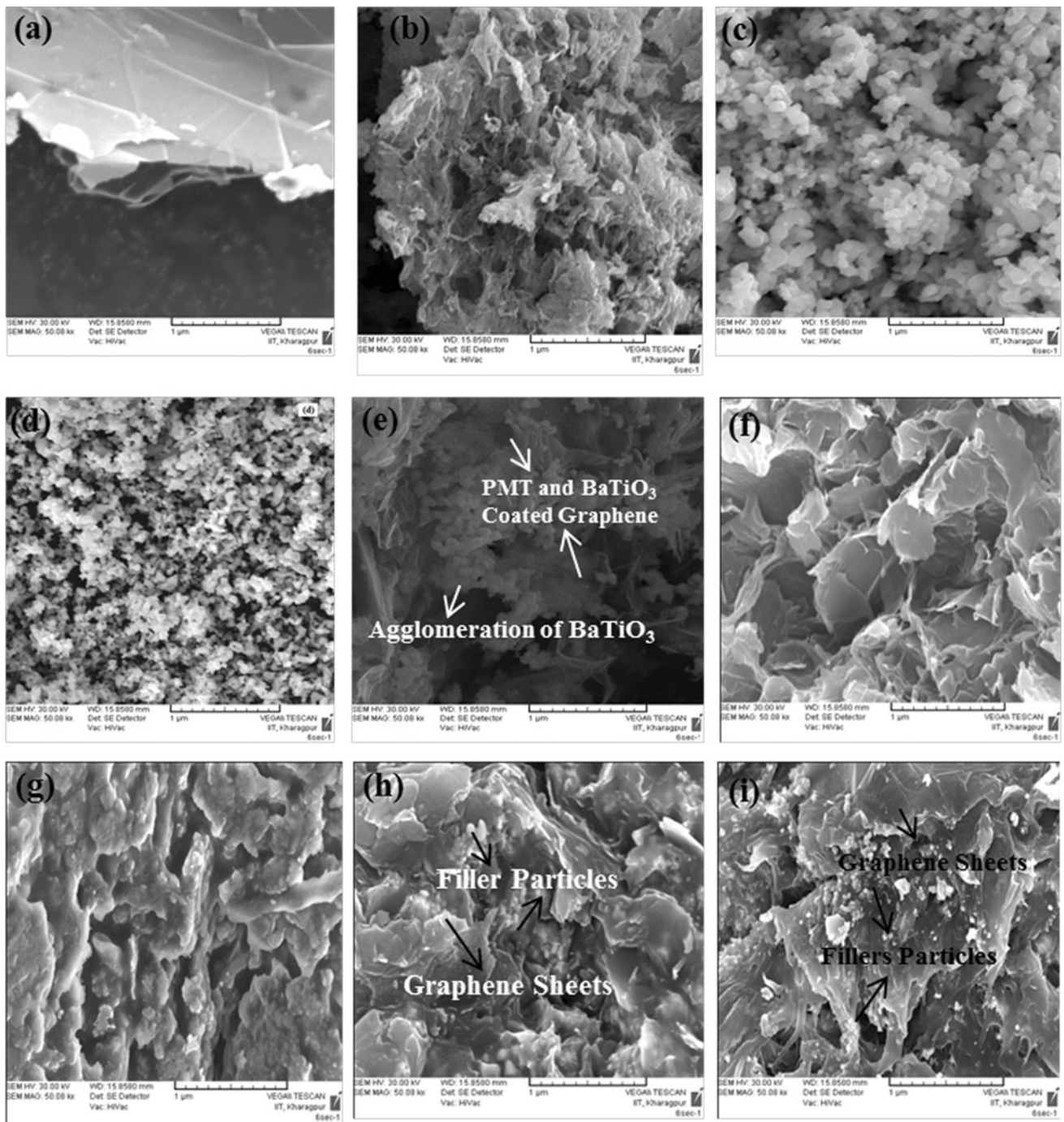


Fig. 3 SEM images of **a** graphene, **b** PMT, **c** BaTiO₃, **d** Fe₃O₄, **e** graphene/PMT/BaTiO₃ nanocomposite and the fractured cross-section of **f** P1, **g** P2, **h** P3 and **i** P4

4.3 Microwave absorbing properties

RAMs absorb microwave radiation and radiates as heat energy. The characteristic electromagnetic parameters of an absorbing material are real and imaginary part of permittivity (ϵ' , ϵ'') and the same for permeability (μ' , μ''). The normalized input impedance (Z) with respect to the

impedance in free space, and reflection loss (RL) are given by the equation [30].

$$z = \sqrt{(\mu_r/\epsilon_r)} \tanh \left[-j \left(\frac{2\pi}{c} \right) (\sqrt{\mu_r \epsilon_r}) fd \right]$$

$$\text{Reflection loss (in dB)} = -20 \log \left[\left| \frac{z-1}{z+1} \right| \right]$$

Fig. 4 EDX study of **a** P3 and **b** P4

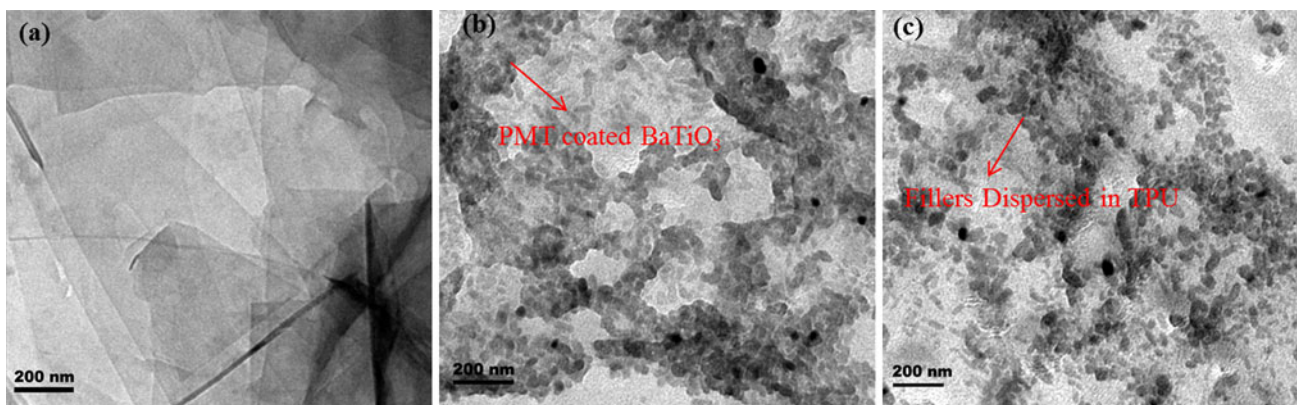
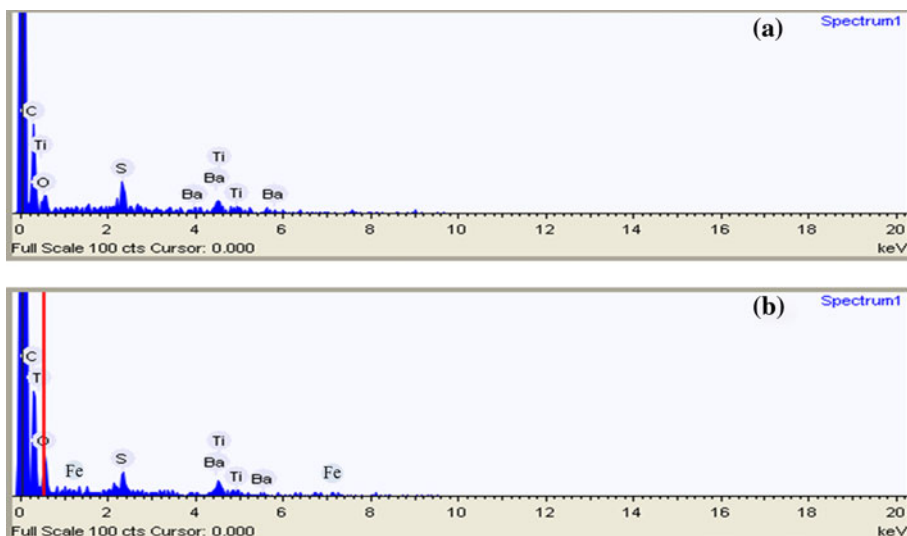
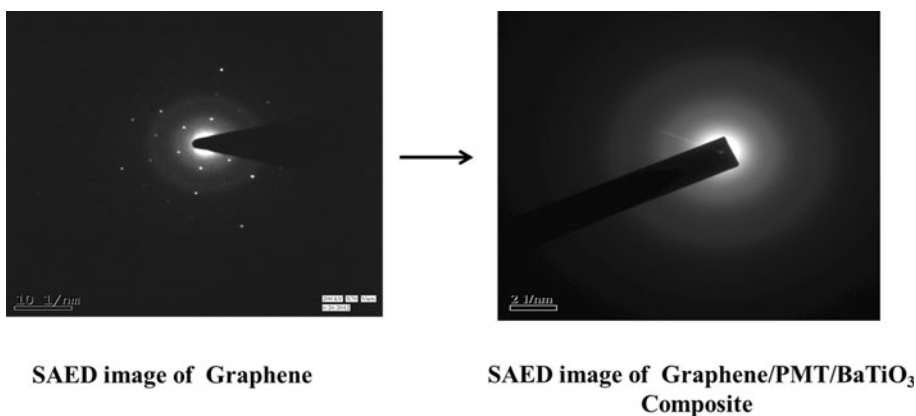


Fig. 5 TEM images of **a** graphene, **b** graphene/PMT/BaTiO₃ nanocomposite and **c** P4

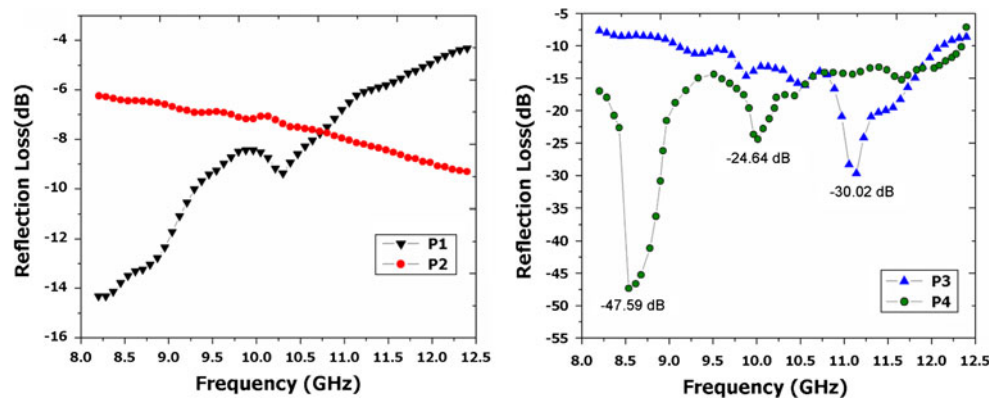
Fig. 6 SAED image of graphene and graphene/PMT/BaTiO₃ nanocomposite



where μ_r and ϵ_r are the relative complex permeability and permittivity of the absorber medium; f and c are the frequency of microwave in free space and the velocity of light, respectively; and d is the sample thickness.

Figure 7 represented the return loss versus frequency plot for P1, P2, P3 and P4. The prepared RAMs showed the absorbing properties in a wide frequency range in the X-band region. P1, P2, P3 and P4 showed the maximum

Fig. 7 Return loss versus frequency plot of P1, P2, P3 and P4



return loss of -14.3 dB at 8.19 GHz, -9.3 dB at 12.39 GHz, -30.02 dB at 11.15 GHz and -47.59 dB at 8.53 GHz respectively. The transmission line theory [31] proposed that the reflectivity of an electromagnetic wave transmits through a medium; depend upon many factors like permittivity, permeability, sample thickness, and electromagnetic wave frequency. Since the frequency of radiation and thickness of sample was same for all samples during measurement, so to explain the difference in absorption ability of the RAMs we studied their permittivity and permeability characteristics which have been explained in detail below under the Sect. 4.3.1. Though graphene and PMT both are conducting but may be due to the flat structure of graphene and presence of highly delocalised π -electron cloud in graphene P1 showed better absorption properties than P2. Some functional groups present in the graphene sheet generated during the modification of graphene may also increase the microwave absorption ability of P1 [20]. Now as all the measurement has been done with 30 % loading of the filler it is very much expensive for P1 because graphene is very costly. So to make it cost effective we prepared a nanocomposite with the combination of graphene and PMT in presence of one dielectric material BaTiO_3 . P3 showed better absorption properties than P1 and P2. P3 showed its microwave absorption property due to the conducting nature of graphene and PMT and dielectric nature of BaTiO_3 as well. That means it is mainly due to the dual loss mechanism of electrical conductivity and dielectric polarization [32]. P3 also can show its microwave absorption property due to dielectric relaxation, interfacial scattering [33] and multiple reflections due to the difference in complex permittivity between graphene and PMT [12]. The dielectric relaxation and polarization were mainly induced by interfacial multipoles, which existed along the boundaries between graphene sheets and PMT [34, 35]. P4 showed the most superior microwave absorbing property among the all four RAMs because additionally it contained a magnetic component Fe_3O_4 which also responsible for microwave

absorption. The mechanism of microwave absorption was discussed below with the help of real and imaginary parts of permittivity and permeability.

4.3.1 Relative complex permittivity and permeability

A RAM mainly showed two types of loss, one is dielectric loss and other one is magnetic loss. Hence, to investigate the possible mechanism of microwave absorption, we determined the real and imaginary parts of complex permittivity (ϵ' , ϵ'') and permeability (μ' , μ'') from the scattering parameters with the help of Nicolson-Ross-Weir (NRW) method [36]. Figure 8a, b shows the real and imaginary parts of complex relative permittivity spectra respectively. Figure 8c, d shows the real and imaginary parts of complex relative permeability. The real part of permittivity (ϵ') refers the amount of energy stored in a material due to an external electric field. The imaginary part of permittivity (ϵ'') is known as loss factor and is a measure of how much energy dissipated or lost. The values of real parts of permittivity (ϵ') for P1 lie from 19.04 to 15.21. The ϵ' for P2 lie from 2.0 to 2.05. The values of ϵ' for P3 lie from 10.87 to 11.02 and for P4, 6.57 to 6.80. The real part of permittivity for P1 follows a decreasing trend with increase in frequency. The effect of frequency on permittivity is directly related to polarization, i.e., as the frequency of the field is raised, the periodic reversal of electric field occurs so quickly that there is no excess ion diffusion in the field direction. Hence, polarization due to charge accumulation decreases, leading to decrease in permittivity value with increasing frequency [37, 38]. The real part of permittivity for P2, P3 and P4 remains almost unaltered with increase in frequency. According to the theory of permittivity, the electric field of electromagnetic wave has the ability to induce two types of electrical currents i.e., conduction and displacement current within the material under the influence of an electromagnetic field. The presence of free electrons for conduction is responsible for conduction current and gives imaginary part of

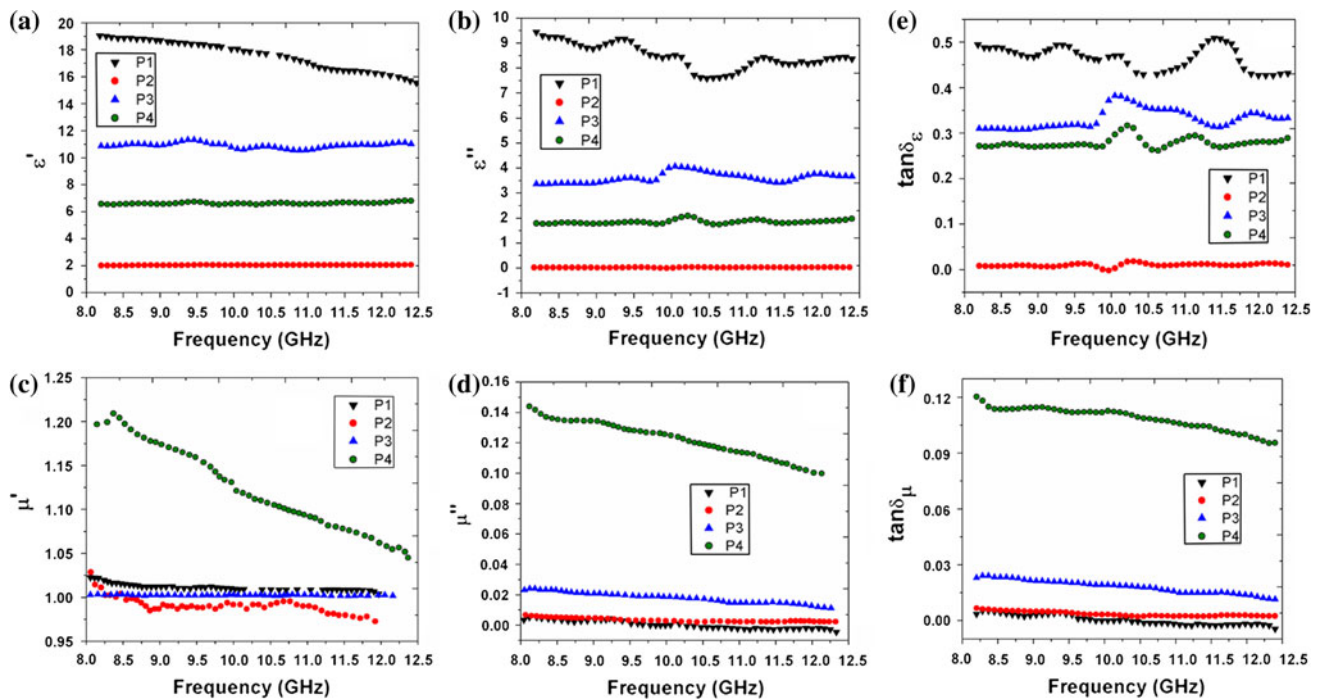


Fig. 8 **a** Real (ϵ') and **b** imaginary (ϵ'') parts of relative complex permittivity, **c** real (μ') and **d** imaginary (μ'') parts of relative complex permeability, **e** loss tangent of relative complex permittivity ($\tan\delta_\epsilon$)

and **f** loss tangent of relative complex permeability ($\tan\delta_\mu$) of the prepared RAMs

permittivity (ϵ''), whereas displacement current arises due to the bound charges, i.e., polarization and gives real part of permittivity (ϵ') [39]. The values of imaginary parts of permittivity (ϵ'') for P1 lie from 9.45 to 8.33. The ϵ'' for P2 is close to 0. The value of ϵ'' for P3 lie from 3.39 to 3.59 and for P4, 1.79 to 1.97 which means all are constant throughout the whole X-band region. The values of μ' and μ'' for P4 lie from 1.19 to 1.03 and 0.14 to 0.09 respectively. The imaginary part of permeability (μ''), for RAMs other than P4, is almost zero and the real part of the same is close to zero and not so impressive. Magnetic losses are mainly due to the hysteresis loss and eddy current loss provided by Fe_3O_4 particle [40]. From the permittivity and permeability data it can be concluded that for P3 dielectric loss is more prominent whereas for P4 magnetic loss is more important. To know the exact loss by each RAM, we have showed the plot of loss tangent against frequency for relative complex permittivity ($\tan\delta_\epsilon$) and permeability ($\tan\delta_\mu$) in the Fig. 8e, f respectively. P1, P2 and P3 are mainly responsible for dielectric loss whereas P4 shows both dielectric and magnetic loss. P3 also showed little bit of magnetic loss which may be due to the impurities present in the material. P1 has better dielectric property among all RAMs which may be due to the high loading percentage of graphene. The loss tangent value of each RAMs supports their microwave absorption property behaviour.

4.4 Thermo gravimetric analysis (TGA)

An effective RAM should have high thermal stability for its application in different fields. Hence, the thermal stability of the RAMs namely P1, P2, P3 and P4 were analyzed by TGA instrument, in Nitrogenous atmosphere. As shown in the Fig. 9, all the four samples showed a similar type of thermal behaviour from 30 to 650 °C. All the samples are quite stable up to above 300 °C. From the inset figure it is clear that the degradation for P2 has started earlier than the other member of this group. Individually all the RAMs showed a constant line after 500 °C. But the weight loss is different for different RAMs. Maximum weight loss for P1, P2, P3 and P4 is 77, 93, 74 and 73 % respectively. Hence, the residual weight of the entire sample excluding P2 is around 30 %. The residual weight for P2 is only 7 % because of the degradation of only polymers. Graphene is thermally stable under this working temperature range, but P1 showed little degradation which may be due to the acid modification of graphene. Higher thermal stability of P3 and P4 may be due to the presence of nanofiller which can provide better interaction among the different components of the nanocomposite. In the TGA plot there are two different degradation zones—one was started around 320 °C and ended around 390 °C, the second degradation was started from 410 °C and ended on around 500 °C. The reason for first degradation is not very

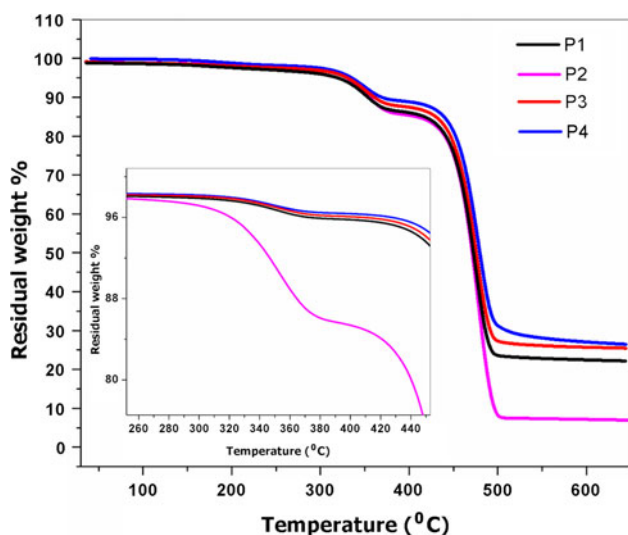


Fig. 9 TGA plot of P1, P2, P3 and P4

clear but it may be due to the presence of some volatile compounds and the sharp second degradation is due to the degradation of TPU. Hence, regarding the thermal stability of the RAMs P1, P3 and P4 is better candidate than P2.

5 Conclusion

In conclusion, graphene and metal oxide based nanocomposites are potential candidates for microwave absorption study. Different nanocomposites were prepared and analysed by different analytical technique to confirm their formation and to study their microwave absorption property. Result shows that P4, Which contain both dielectric and magnetic material, is more promising candidate among all. In case of P3, only dielectric loss is important but in P4 proper matching of dielectric and magnetic component helps to make it potential RAM. P1 and P2 become lossy mainly due to the conductivity of graphene and PMT respectively. Flat structure of graphene also has some impact on the observed result of graphene and its nanocomposites. P1, P3 and P4 have high thermal stability which demanded that they can be used as a RAM for high temperature application. Hence, graphene and its nanocomposite with metal oxide have high impression on this particular application and can be used very effectively in future.

Acknowledgments The authors are thankful to CSIR, New Delhi, INDIA for their financial support in this work. Authors are also thankful to IIT Kharagpur, India.

References

1. L. Zhou, W. Zhou, J. Su, F. Luo, D. Zhu, Y. Dong, *Appl. Surf. Sci.* **258**, 2691–2696 (2012)

2. J.M. Zhao, W.X. An, D.A. Li, X. Yang, *Syn. Met.* **161**, 2144–2148 (2011)
3. Y. Lu, Q. Liang, L. Xue, *Appl. Surf. Sci.* **258**, 4782–4787 (2012)
4. X. Chen, G. Wang, Y. Duan, S. Liu, *J. Appl. Phys.* **40**, 1827–1830 (2007)
5. T. Maeda, S. Sugimoto, T. Kagotani, N. Tezuka, K. Inomata, *J. Magn. Magn. Mater.* **281**, 195–205 (2004)
6. Z.G. Fan, G.H. Luo, Z.G. Zhang, L. Zhou, F. Wei, *Mat. Sci. Eng. B-SOLID.* **132**, 85–89 (2006)
7. J.L. Wojkiewicz, S. Fauveaux, J.L. Miane, *Syn. Met.* **135**, 127–128 (2003)
8. M.A. Soto-Oviedo, O.A. Araujo, R. Faez, M.C. Rezende, M.A. De Paoli, *Syn. Met.* **156**, 1249–1255 (2006)
9. X. Du, I. Skachko, A. Barker, E.Y. Andrei, *Nat. Nanotechnol.* **3**, 491 (2008)
10. R. Hao, W. Qian, L.H. Zhang, Y.L. Hou, *Chem. Commun.* **48**, 6576–6578 (2008)
11. Z. Ma, C. Cao, J. Yuan, Q. Liu, J. Wang, *Appl. Surf. Sci.* **258**, 7556–7561 (2012)
12. X. Bai, Y. Zhai, Y. Zhang, *J. Phys. Chem. C* **115**, 11673–11677 (2011)
13. M. Zhanga, H. Zhangb, G. Zengc, *Adv. Mat. Res.* **194**, 520–523 (2011)
14. A. Saib, L. Bednarz, R. Daussin, C. Bailly, X. Lou, J.M. Thomassin, C. Pagnouille, C. Detrembleur, R. Jerome, I. Huynen, *IEEE. T. Micro. Theory* **54**, 2745–2754 (2006)
15. L.J. Deng, M.G. Han, *Appl. Phys. Lett.* **91**, 023119-1 (2007)
16. R.T. Lv, A.Y. Cao, F.Y. Kang, W.X. Wang, J.Q. Wei, J.L. Gu, K.L. Wang, D.H. Wu, *J. Phys. Chem. C* **111**, 11475–11479 (2007)
17. Y. Li, Y. Huang, S. Qi, L. Niu, Y. Zhang, Y. Wu, *Appl. Surf. Sci.* **258**, 3659–3666 (2012)
18. C. Wang, X. Han, P. Xu, X. Zhang, Y. Du, S. Hu, J. Wang, X. Wang, *Appl. Phys. Lett.* **98**, 072906-1 (2011)
19. J. Liang, Y. Wang, Y. Huang, Y. Ma, Z. Liu, J. Cai, C. Zhang, H. Gao, Y. Chen, *Carbon* **47**, 922 (2009)
20. Y. Zhan, F. Meng, X. Yang, R. Zhao, X. Liu, *Mater. Sci. Eng. B-Adv.* **176**, 1333–1339 (2011)
21. W. Zhou, X. Hu, X. Bai, S. Zhou, C. Sun, J. Yan, P. Chen, *ACS Appl. Mater. Interfaces* **3**, 3839–3845 (2011)
22. S. Ni, X. Wang, G. Zhou, F. Yang, J. Wang, D.J. He, *J. Alloys, Compound* **489**, 252–256 (2010)
23. S.B. Ni, S.M. Lin, Q.T. Pan, F. Yang, K. Huang, D.Y. He, *J. Phys. D Appl. Phys.* **42**, 055004 (2009)
24. A. Laforgue, P. Simon, C. Sarrazin, J.F. Fauvarque, *J. Power Sour.* **80**, 142–148 (1999)
25. M. Mastragostino, C. Arbizzani, F. Sovai, *J. Power Sour.* **97–98**, 812–815 (2001)
26. S. Das, A. Mandal, C.K. Das, *Nano Trends: J. Nanotechnol. Appl.* **11**, 01–07 (2011)
27. C.K. Das, A. Mandal, *J. Mater. Sci. Res.* **1**, 45–53 (2012)
28. W. Qian, Z. Chen, M. Eastman, S. Cottingham, B. Manhat, A. Goforth, J. Jiao, *Ultramicroscopy.* (2011). doi:10.1016/j.ultramic.2011.11.010
29. J. Deng, Y. Peng, C. He, X. Long, P. Li, A.S.C. Chan, *Polym. Int.* **52**, 1182–1187 (2003)
30. Y.R. Gang, *J. Magn. Magn. Mater.* **323**, 1805–1810 (2011)
31. E. Michielssen, J. Sajer, S. Ranjithan, R. Mitra, *IEEE. T. Micro. Theory* **41**, 1024–1030 (1993)
32. D. Micheli, C. Apollo, R. Pastore, M. Marchetti, *Compos. Sci. Technol.* **70**, 400 (2010)
33. X.Y. Fang, M.S. Cao, X.L. Shi, Z.L. Hou, W.L. Song, J. Yuan, *J. Appl. Phys.* **107**, 054304 (2010)
34. Y.J. Chen, M.S. Cao, T.H. Wang, Q. Wan, *Appl. Phys. Lett.* **84**, 3367–3370 (2004)

35. D.L. Zhao, X. Li, Z.M. Shen, *Mater. Sci. Eng. B-Adv.* **150**, 105 (2008)
36. A.L. Paula, M.C. Rezende, J.J. Barroso, *J. Aeros. Technol. Mange.* **3**, 59–64 (2011)
37. V. Raja, A.K. Sharma, V.V.R. Narasimha, *Mater. Lett.* **58**, 3242–3247 (2004)
38. A. Ohlan, K. Singh, A. Chandra, S.K. Dhawan, *ACS Appl. Mater. Interface* **2**, 927–933 (2010)
39. A. Gupta, V. Choudhary, *Compos. Sci. Technol.* **71**, 1563–1568 (2011)
40. Y.F. Zhua, L. Zhangb, T. Natsukic, Y.Q. Fud, Q.Q. Ni, *Syn. Met.* **162**, 337–343 (2012)